scientific reports

Check for updates

OPEN

Radiative mixed convection flow of maxwell nanofluid over a stretching cylinder with joule heating and heat source/sink effects

Saeed Islam[1,2], Arshad Khan[3], Poom Kumam[4,5]✉, Hussam Alrabaiah[6,7], Zahir Shah[8]✉, Waris Khan[9], Muhammad Zubair[10] & Muhammad Jawad[10]

This work analyses thermal effect for a mixed convection flow of Maxwell nanofluid spinning motion produced by rotating and bidirectional stretching cylinder. Impacts of Joule heating and internal heat source/sink are also taken into account for current investigation. Moreover, the flow is exposed to a uniform magnetic field with convective boundary conditions. The modeled equations are converted to set of ODEs through group of similar variables and are then solved by using semi analytical technique HAM. It is observed in this study that, velocity grows up with enhancing values of Maxwell, mixed convection parameters and reduces with growing values of magnetic parameter. Temperature jumps up with increasing values of heat source, Eckert number, Brownian motion, thermophoresis parameter and jumps down with growing values of Prandtl number and heat sink. The concentration is a growing function of thermophoresis parameter and a reducing function of Brownian motion and Schmidt number.

Symbols

$u,\ w$	Axial and radial velocity components $\left(\mathrm{ms}^{-1}\right)$
T_∞	Ambient fluid temperature (K)
C_∞	Ambient fluid concentration
D_B	Brownian diffusion coefficient $\left(\mathrm{m^2 s^{-1}}\right)$
N_b	Brownian motion parameter
N_r	Buoyancy ratio
l	Characteristic length (m)
T	Dimensional temperature (K)
C	Dimensional concentration
Ec_1	Eckert number for cylinder's stretching
Ec_2	Eckert number for cylinder's rotation
M	Hartman number

[1]Faculty of Mathematics & Statistics, Ton Duc Thang University, Ho Chi Minh City 70000, Vietnam. [2]Informetrics Research Group, Ton Duc Thang University, Ho Chi Minh City 70000, Vietnam. [3]College of Aeronautical Engineering, National University of Sciences and Technology (NUST), Sector H-12, Islamabad 44000, Pakistan. [4]KMUTT Fixed Point Research Laboratory, Room SCL 802 Fixed Point Laboratory, Science Laboratory Building, Department of Mathematics, Faculty of Science, King Mongkut's University of Technology Thonburi (KMUTT), 126 Pracha-Uthit Road, Bang Mod, Thrung Khru, Bangkok 10140, Thailand. [5]Department of Medical Research, China Medical University Hospital, China Medical University, Taichung 40402, Taiwan. [6]College of Engineering, Al Ain University, Al Ain 64141, UAE. [7]Department of Mathematics, Tafila Technical University, Tafila 66110, Jordan. [8]Department of Mathematics, University of Lakki Marwat, Lakki Marwat 28420, Khyber Pakhtunkhwa, Pakistan. [9]Department of Mathematics, Division of Science and Technology, University of Education Lahore, Lahore 54770, Pakistan. [10]Department of Mathematics, Abdul Wali Khan University, Mardan 23200, Khyber Pakhtunkhwa, Pakistan. ✉email: poom.kum@kmutt.ac.th; zahir.1987@yahoo.com

nature research

1

T_f	Heated fluid temperature (K)
C_f	Heated fluid concentration
Nu_z	Local Nusselt number
Sh_z	Local Sherwood number
Re_z	Local Reynolds number
B_0	Magnetic field strength $\left(NmA^{-1}\right)$
k_m	Mass transfer coefficient
D_m	Molecular diffusivity of species concentration
Pr	Prandtl number
U_0	Reference velocity $\left(ms^{-1}\right)$
Re	Reynolds number
Sc	Schmidt number
h_m	Surface mass flux $\left(W\ m^{-2}\right)$
q_w	Surface heat flux $\left(W\ m^{-2}\right)$
k	Thermal conductivity $\left(W\ K^{-1}m^{-1}\right)$
D_T	Thermophoretic diffusion coefficient $\left(m^2s^{-1}\right)$
N_t	Thermophoresis parameter

Greek symbols

γ	Curvature parameter
β_T	Coefficient of thermal expansion
γ_2	Concentration Biot number
ϕ	Dimensionless fluid concentration
θ	Dimensionless temperature
ρ	Density $\left(kg\ m^{-3}\right)$
δ	Heat generation/absorption parameter
υ	Kinematic viscosity $\left(m^2s^{-1}\right)$
β_1	Maxwell parameter
λ	Mixed convection parameter
η	Similarity variable
α_1	Thermal diffusivity $\left(m\ s^{-1}\right)$
γ_1	Thermal Biot number

Superscript

$'$	Prime denotes derivative w. r. t. η

Abbreviations

HAM	Homotopy analysis method
ODEs	Ordinary differential equations
RK-4	Runge–Kutta method of order four
MHD	Magnetohydrodynamics
PDEs	Partial differential equations

Recently, due to rapid development in modern industry, the scientists and researchers are forced to search such techniques and methods those are used for enhancement of heat transmission in heat exchanger equipment. In order to fulfill these requirements, scientists and researchers developed a new type of fluid, named as nanofluid and is used for commercial and industrial applications. This type of fluid is prepared by suspending nanoparticles in some base/pure fluid. Experiments have shown that combination of nanoparticles with base fluid enhances the coefficient of heat transmission of nanofluids. The usual materials used for nanoparticles are Al_2O_3, Cu, TiO_2, Ag etc. The quantity of nanoparticles was first suggested by Choi[1] for augmenting thermal properties of pure fluid. Later, the subject of nanofluid was developed by a number of scientists and researchers. Elahi et al.[2] examined mixed convection flow for nanoparticles on a porous surface by considering various shapes of nanoparticles. Dogonchi along with Ganji[3] studied magnetic heat transfer for nanofluid past a stretched surface and noticed an augmentation in flow characteristics with growing values of thermal radiations. These two authors[4] have also discussed MHD nanofluid flow and transfer of heat by using Joule heating between two surfaces. The reader can further study about nanofluid in ref[5–8].

For mixed convection flow, the difference of concentration and temperature results in buoyancy forces. These flows are considerable in various applications at industrial level. The collective effects of mass and heat transmission in mixed convection flows have extraordinary importance for complex engineering problems. Mukhopadhyay[9] has discussed time-dependent mixed convection fluid flow with transmission of heat past a permeable stretched surface using slip condition. In this study, the author has solved the modeled problem numerically and has determined that, with augmentation of unsteadiness parameter there was a corresponding reduction in both temperature and velocity. Hayat et al.[10] have examined mixed convection flow using convective boundary conditions past a stretched sheet. In this investigation, the authors have discussed numerical values for Nusselt number and skin-friction and have also compared their results with existing solutions available in literature. Turkyilmazoglu[11] has analytically studied solutions for mixed convection heat transmission

of electrically conducted, viscoelastic fluid flowpast a stretchedsurface using Dufour and Soret effects. Shehzad et al.[12] have discussed characteristics of heat and mass transmission for 3-D flow of Oldroyd-B fluid past a bi-directional stretchedsurfaceusing radiation effects. Xu and Pop[13] have analyzed mixed convective flow for nanofluid past a stretched sheet using gyrotactic microorganisms and nanoparticles with uniform free stream. Moreover, tremendous investigation has also been carried out by Sankar et al.[14–19] in the area of convective heat transfer by using various geometries and flow conditions. Their work has comprised of numerical as well as analytical investigations.

Study of heat transmission for linear and non-linear fluids plays very considerable role in various engineering processes for instance, electronic equipment cooling, extrusion process, inconservation of energy in nuclear reactor and cooling of nuclear reactor etc. Heat transport induced by rotating and stretching surfaces in viscoelastic fluid has a significant importance in plastic manufacturing because the final products quality is mainly dependent on heat transport. Numerous investigations have been carried out by the researchers for prediction of heat transport in flow of fluidfor rotating and stretching surfaces. Mustafa et al.[20] have studied transmission of mass and heatamid two plates. They have examined in this study that, augmentation in magnitude of Schmidt number enhances the values of local Sherwood number while reduces the concentration profile. Kumar and Nath[21] have carried out the analytical study of time dependent 3D MHD boundary layer flow and heat transmission for stretched plane surface. In this study, the authors have showed that analytical series solution is very much precise in the complete domain for all values of time. Alizadeh et al.[22] have discussed MHD micropolar flow of fluid in a conduit filled with nanoparticles using thermal effects. Ashorynejad et al.[23] have investigated heat transmission of MHD nanofluid past a stretching cylinder. In this investigation, the authors have solved the system of modeled ODEs by RK-4 method. Seth et al.[24,25] have investigated Casson fluid flow with Newtonian heating and thermo diffusion effects using porous and non-Darcy porous media. Tripathi et al.[26] have discussed double diffusive flow for hydromagneticnanofluid through a rotating channel using Hall Effect and viscous dissipation. Arifuzzaman et al.[27] have discussed transmission of heat and mass for MHD fourth-grade radiative fluid flow over a porous plate using chemical reaction.

Fluid flow over a stretching flat plate or cylinder has achieved consideration from numerous researchers because of its significant applications at industrial level, such as liquid film for condensation procedure, growing of crystals, foods and papers manufacturing, glass fabrication and polymer extrusion etc. Due to its importance, many researchers diverted their attention towards the flow past a stretching flat plate or cylinder. Crane[28] has studied the flow past a stretched sheet. Wang and Ng[29] have discussed slip flow past a stretched cylinder. In this study, they have used suitable set of similarity transformation to transform the governing PDEs to set of non-linear ODEs. They have further transformed this set of non-linear ODEs to a simple form by using compressed variable and then solved this new system by using numerical integration. The main outcome of their study was that, they have determined that the magnitudes of shear stress and velocities are greatly trimmed down by slip flow. Bhattacharyya et al.[30] havediscussedsimulation of Cattaneo-Christov heat flux for single as well as multi walled CNTs (Corbon Nanotubes) between two stretched rotating coaxial disks. Seth et al.[31] studied entropy generation for flow of hydromagneticnanofluidover non-linear stretched surface using Navier's velocity slip with convective heat transfer. The readers can further study about stretching flows by using different geometries in ref[32–37].

In this work we shall endeavor to

i. Discuss mixed convection flow for Maxwell nanofluid with transfer of thermal energy over a stretching and rotating cylinder.
ii. Analyze heat transmission using Joule heating with heat generation/absorption in nanofluid flow.

The modeled problem will then be transformed to set of ODEs employing group of similar variables. The resultant set of ODEs will be solved by using HAM[38–40]. The behavior of different substantial parameters will be examined and discussed graphically. Moreover, a comparison will also be carried out for validation of current work with the results as available in literatur[46].

Physical and mathematical model

In this section we shall firstgive physical description of the problem. Then the mathematical formulation of problem and suitable set of dimensionless variables will be introduced. Moreover, some physical parameters will also be defined along with mathematical representations in this section.

Physical description. For current flow problem the following assumptions are considered

i. Take a mixed convection flow for Maxwell nanofluid over a stretching and rotating cylinder of radius a.
ii. Magnetic field of intensity B_0 is applied to flow system.
iii. Let $V = [u, v, w]$ be velocity field with u, v and w as its components along z, θ and r-axes respectively (See Fig. 1). Axis of cylinder is taken along z-axis and radial direction is along r-axis.
iv. Maxwell nanofluid model along with thermophoresis and Brownian motion effects are considered for flow problem.
v. Temperature and concentration at surface of cylinder aretaken as T_w, C_w while these quantities at free stream are T_∞, C_∞. In concentration equation the chemical reaction is assumed to be overlooked.
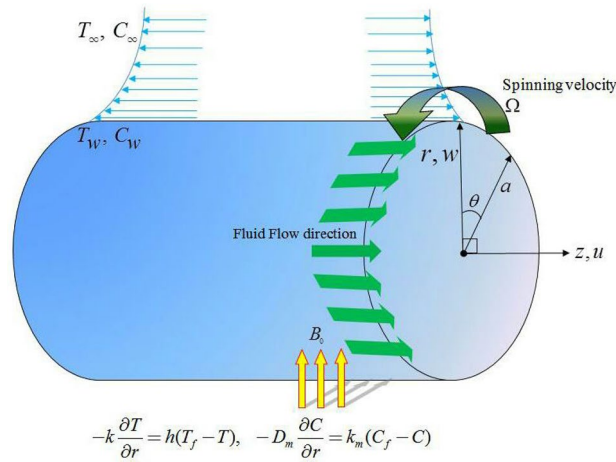
Figure 1. Geometry of flow problem.

Mathematical description. Considering all assumptions as stated in "Physical description" section the mathematical representation for flow system takes the form[41–45]

$$\frac{\partial u}{\partial z} + \frac{w}{r} + \frac{\partial w}{\partial r} = 0 \tag{1}$$

$$u\frac{\partial u}{\partial z} + w\frac{\partial u}{\partial r} + \lambda_1\left[w^2\frac{\partial^2 u}{\partial r^2} + 2uw\frac{\partial^2 u}{\partial r\partial z} + u^2\frac{\partial^2 u}{\partial z^2}\right] = -\frac{1}{\rho}\frac{\partial p}{\partial z} + \upsilon\left[\frac{1}{r}\frac{\partial u}{\partial r} + \frac{\partial^2 u}{\partial r^2}\right]$$
$$-\frac{\sigma B_0^2}{\rho}\left(\lambda_1 w\frac{\partial u}{\partial r} + u\right) + g\left[\frac{\rho^* - \rho}{\rho}(C - C_\infty) + \beta_T(T - T_\infty)(1 - C_\infty)\right], \tag{2}$$

$$w\frac{\partial T}{\partial r} + u\frac{\partial T}{\partial z} = \alpha_1\left[\frac{1}{r}\frac{\partial T}{\partial r} + \frac{\partial^2 T}{\partial r^2}\right] + \tau\left[\frac{D_T}{T_\infty}\left(\frac{\partial T}{\partial r}\right)^2 + D_B\frac{\partial T}{\partial r}\frac{\partial C}{\partial r}\right]$$
$$+\frac{Q_0}{\rho c_p}(T - T_\infty) + \frac{\sigma B_0^2}{\rho c_p}(v^2 + u^2) \tag{3}$$

$$w\frac{\partial C}{\partial r} + u\frac{\partial C}{\partial z} = D_B\left[\frac{\partial^2 C}{\partial r^2} + \frac{1}{r}\frac{\partial C}{\partial r}\right] + \frac{D_T}{T_\infty}\left[\frac{1}{r}\frac{\partial T}{\partial r} + \frac{\partial^2 T}{\partial r^2}\right] \tag{4}$$

Subjected BCs are

$$u = U = \frac{U_0 z}{l}, \; w = 0, \; -k\frac{\partial T}{\partial r} = h\left(T_f - T\right), -Dm\frac{\partial C}{\partial r} = k_m\left(C_f - C\right) \; at \; r = a \tag{5}$$

$$C \to C_\infty, \; u \to 0, \; T \to T_\infty \quad as \; r \to \infty$$

Group of dimensionless variables is

$$\psi = (U\upsilon z)^{1/2} af(\eta), \; \phi(\eta) = \frac{C - C_\infty}{C_f - C_\infty}, \; \theta(\eta) = \frac{T - T_\infty}{T_f - T_\infty}, \; \eta = \frac{(r^2 - a^2)}{2a}\sqrt{\frac{U}{\upsilon z}} \tag{6}$$

Making use of Eq. (6) in Eqs. (1–5) we have

$$(2\gamma\eta + 1)f''' + ff'' + 2\gamma f'' - f'^2 - \beta_1 \mathrm{Re}\left(2f^2 f''' + \frac{f^2 f''}{\eta} - 4ff'f''\right)$$
$$+ \lambda(\theta + N_r\phi) - M(f' - \beta_1 ff'') = 0 \tag{7}$$

$$(2\gamma\eta + 1)\theta'' + \mathrm{Pr}N_b(2\gamma\eta + 1)\theta'\phi' + \mathrm{Pr}f\theta' + \mathrm{Pr}\,M\left(Ec_1 f'^2 + Ec_2 g\right)$$
$$+ \mathrm{Pr}\,N_t(2\gamma\eta + 1)\theta'^2 + \delta\,\mathrm{Pr}\,\mathrm{Re}\theta = 0 \tag{8}$$

4

$$(1 + 2\gamma\eta)\phi'' + 2\gamma\phi' + Scf\phi' + \frac{N_t}{N_b}[(1 + 2\gamma\eta)\theta'' + 2\gamma\theta'] = 0 \tag{9}$$

Subjected BCs are now

$$f(0) = 0, \ f'(0) = 1, \quad \theta'(0) = -\gamma_1[1 - \theta(0)], \ \phi'(0) = -\gamma_2[1 - \phi(0)],$$
$$f'(\infty) = 0, \quad \theta(\infty) = 0, \quad \phi(\infty) = 0 \tag{10}$$

In above equations we have $\gamma = \left(\frac{\upsilon l}{U_0 a^2}\right)^{1/2}$ = curvature parameter, $N_r = \frac{(\rho^* - \rho)\Delta C}{\rho\beta_T \Delta T (1 - \phi_\infty)}$ = Buoyancy ratio, $M = \frac{\sigma B_0^2 l}{\rho U_0}$ = Hartman number, $N_b = \frac{\tau D_B \Delta C}{\upsilon}$ = Brownian motion parameter, $\Pr = \frac{\upsilon}{\alpha}$ = Prandtl number, $\lambda = \frac{gl^2 \beta_T (1 - C_\infty)\Delta T}{U_0^2 z}$ = Mixed convection parameter, $Sc = \frac{\upsilon}{D_B}$ = Schmidt number, $N_t = \frac{\tau D_T \Delta T}{T_\infty \upsilon}$ = Thermophoresis parameter, $Ec_1 = \frac{u_w^2}{c_p \Delta T}$ = Eckert number for cylinder's stretching, $Ec_2 = \frac{v_w^2}{c_p \Delta T}$ = Eckert number for cylinder's rotation, $\beta_1 = \lambda_1 a$ = Maxwell parameter and $\delta = \frac{Q_0}{\rho c_p a}$ = Heat generation/absorption parameter.

Some quantities of importance.   For modeled problem Nusselt and Sherwood numbers are given by

$$Nu_z = \frac{zq_w}{k(T_f - T_\infty)}, \qquad Sh_z = \frac{zh_m}{D_B(C_f - C_\infty)} \tag{11}$$

In Eq. (11) h_m and q_w are defined as

$$h_m = \left(-D_B \frac{\partial C}{\partial r}\right)_{r=a} \ , \qquad q_w = \left(-k \frac{\partial T}{\partial r}\right)_{r=a} \tag{12}$$

Making use of Eq. (6) in Eq. (11) we have

$$Nu_z(\mathrm{Re}_z)^{-1/2} = -\theta'(0), \qquad Sh_z(\mathrm{Re}_z)^{-1/2} = -\phi'(0) \tag{13}$$

Solution of problem

In current work **s**emi analytical method HAM determines solution for resultant set of ODEs as given in Eqs. (7–9) by applying the boundary conditions as stated in Eq. (10). The initial guess for the specified equations is stated below

$$f_0 = 1 - e^{-\eta}, \ \Theta_0 = \frac{\gamma_1}{1 + \gamma_1} e^{-\eta} \ , \ \Phi_0(\eta) = \frac{\gamma_2}{1 + \gamma_2} e^{-\eta} \tag{14}$$

The linear operators are stated as follows

$$L_f(f) = f''' - f', \ L_\Theta(\Theta) = \theta'' - \theta, \ L_\Phi(\Phi) = \phi'' - \phi \tag{15}$$

$$
\begin{aligned}
&L_{\widehat{f}}(e_1 \ + \ e_2 e^\eta \ + \ e_3 e^{-\eta}) = 0, \\
\text{With} \quad &L_{\widehat{\theta}}(e_4 e^\eta \ + \ e_4 e^{-\eta}) = 0, \\
&L_{\widehat{\phi}}(e_6 e^\eta \ + \ e_7 e^{-\eta}) = 0
\end{aligned}
\tag{16}
$$

In Eq. (16) $e_i (for \ i = 1, 2, \ldots, 7)$ are constants.
Further

$$N_{\widehat{f}}\left[\widehat{f}(\eta; \zeta), \widehat{\theta}(\eta; \zeta), \widehat{\phi}(\eta; \zeta)\right] = (2\gamma\eta \ + \ 1)\widehat{f}_{\eta\eta\eta} + 2\gamma\widehat{f}_{\eta\eta} + \widehat{f}\widehat{f}_{\eta\eta} - \widehat{f}_\eta^2$$
$$- \beta_1 \mathrm{Re}\left(\frac{\widehat{f}^2 \widehat{f}_{\eta\eta}}{\eta} + 2\widehat{f}^2 \widehat{f}_{\eta\eta\eta} - 4\widehat{f}\widehat{f}_\eta\widehat{f}_{\eta\eta}\right) - M\left(\widehat{f}_\eta - \beta_1\widehat{f}\widehat{f}_{\eta\eta}\right) + \lambda\left(\widehat{\theta}_\xi + N_r\widehat{\phi}\right) \tag{17}$$

$$N_{\widehat{\theta}}\left[\widehat{f}(\eta; \zeta), \ \widehat{\theta}(\eta; \zeta), \ \widehat{\phi}(\eta; \zeta)\right] = (2\gamma\eta \ + \ 1)\widehat{\theta}_{\eta\eta} + \Pr\widehat{f}\widehat{\theta}_\eta + \Pr N_b(2\gamma\eta \ + \ 1)\widehat{\phi}_\eta\widehat{\theta}_\eta$$
$$+ \Pr M\left(Ec_1\widehat{f}_\eta^2 \ + \ Ec_2\widehat{g}\right) + \Pr N_t(2\gamma\eta \ + \ 1)\widehat{\theta}_\eta^2 \ + \ \delta \Pr \mathrm{Re}\widehat{\theta} \tag{18}$$

$$N_{\widehat{\phi}}\left[\widehat{\phi}(\eta;\zeta),\widehat{f}(\eta;\zeta),\widehat{\theta}(\eta;\zeta)\right] = (1+2\gamma\eta)\widehat{\phi}_{\eta\eta} + Sc\widehat{f}\,\widehat{\phi}_{\eta} + 2\gamma\widehat{\phi}_{\eta}$$
$$+ \frac{N_t}{N_b}\left[(1+2\gamma\eta)\widehat{\theta}_{\eta\eta} + 2\gamma\widehat{\theta}_{\eta}\right] \tag{19}$$

For Eqns. (7–9) the 0th-order system is written as

$$(1-\zeta)L_{\widehat{f}}\left[\widehat{f}(\eta;\zeta) - \widehat{f}_0(\eta)\right] = p\hbar_{\widehat{f}}\,N_{\widehat{f}}\left[\widehat{f}(\eta;\zeta),\widehat{\theta}(\eta;\zeta),(\eta;\zeta)\right] \tag{20}$$

$$(1-\zeta)L_{\widehat{\theta}}\left[\widehat{\theta}(\eta;\zeta) - \widehat{\theta}_0(\eta)\right] = p\hbar_{\widehat{\theta}}\,N_{\widehat{\theta}}\left[\widehat{f}(\eta;\zeta),\ \widehat{\theta}(\eta;\zeta),\widehat{\phi}(\eta,\zeta)\right] \tag{21}$$

$$(1-\zeta)L_{\widehat{\phi}}\left[\widehat{\phi}(\eta;\zeta) - \widehat{\phi}_0(\eta)\right] = p\hbar_{\widehat{\phi}}\,N_{\widehat{\phi}}\left[\widehat{\phi}(\eta;\zeta),\ \widehat{f}(\eta;\zeta),\ \widehat{\theta}(\eta;\zeta)\right] \tag{22}$$

For subjected BCs we have

$$\left.\widehat{f}(\eta;\zeta)\right|_{\eta=0} = 0, \qquad \left.\frac{\partial\widehat{f}(\eta;\zeta)}{\partial\eta}\right|_{\eta=0} = 1, \qquad \left.\frac{\partial\widehat{\theta}(\eta;\zeta)}{\partial\eta}\right|_{\eta=0} = -\gamma_1\left[1 - \left.\widehat{\theta}(\eta;\zeta)\right|_{\eta=0}\right],$$

$$\left.\frac{\partial\widehat{\phi}(\eta;\zeta)}{\partial\eta}\right|_{\eta=0} = -\gamma_2\left[1 - \left.\widehat{\phi}(\eta;\zeta)\right|_{\eta=0}\right], \tag{23}$$

$$\left.\frac{\partial\widehat{f}(\eta;\zeta)}{\partial\eta}\right|_{\eta=\infty} = 0, \qquad \left.\widehat{\theta}(\eta;\zeta)\right|_{\eta=\infty} = 0, \qquad \left.\widehat{\phi}(\eta;\zeta)\right|_{\eta=\infty} = 0$$

When $\zeta = 0$ and $\zeta = 1$ we have (here $\zeta \in [0,1][0,1]$)

$$\widehat{f}(\eta;1) = \widehat{f}(\eta), \widehat{\theta}(\eta;1) = \widehat{\theta}(\eta), \widehat{\phi}(\eta;1) = \widehat{\phi}(\eta), \tag{24}$$

Taylor's expansion for $\widehat{f}(\eta;\zeta), \widehat{\theta}(\eta;\zeta)$ and $\widehat{\phi}(\eta;\zeta)$ about $\zeta = 0$

$$\widehat{f}(\eta;\zeta) = \widehat{f}_0(\eta) + \sum_{n=1}^{\infty}\widehat{f}_n(\eta)\zeta^n$$
$$\widehat{\theta}(\eta;\zeta) = \widehat{\theta}_0(\eta) + \sum_{n=1}^{\infty}\widehat{\theta}_n(\eta)\zeta^n \tag{25}$$
$$\widehat{\phi}(\eta;\zeta) = \widehat{\phi}_0(\eta) + \sum_{n=1}^{\infty}\widehat{\phi}_n(\eta)\zeta^n$$

$$\widehat{f}_n(\eta) = \frac{1}{n!}\left.\frac{\partial\widehat{f}(\eta;\zeta)}{\partial\eta}\right|_{p=0}, \widehat{\theta}_n(\eta) = \frac{1}{n!}\left.\frac{\partial\widehat{\theta}(\eta;\zeta)}{\partial\eta}\right|_{p=0}, \widehat{\phi}_n(\eta) = \frac{1}{n!}\left.\frac{\partial\widehat{\phi}(\eta;\zeta)}{\partial\eta}\right|_{p=0}. \tag{26}$$

With BCs as

$$\widehat{f}(0) = 0, \widehat{f}'(0) = 1, \widehat{\theta}'(0) = -\gamma_1\left[1 - \widehat{\theta}(0)\right], \widehat{\phi}'(0) = -\gamma_2\left[1 - \widehat{\phi}(0)\right] \tag{27}$$

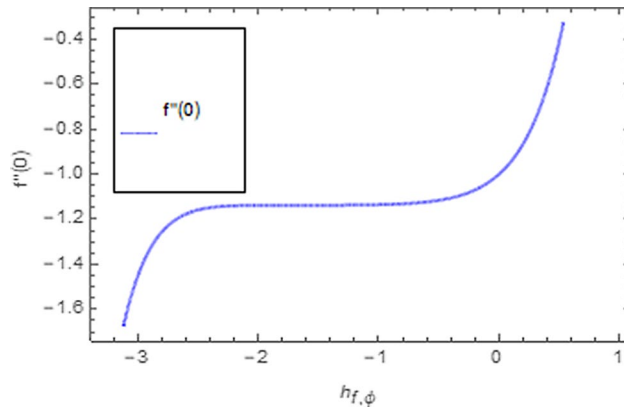$$\widehat{f}'(\infty) = 0, \widehat{g}(\infty) = 0, \widehat{\theta}(\infty) = 0, \widehat{\phi}(\infty) = 0,$$

Figure 2. $h-$ curve for $f'(\eta)$.

Now

$$\Re_n^{\widehat{f}}(\eta) = 2\left(1+\frac{1}{\lambda}\right)f'''_{n-1} + 2\gamma\widehat{f''}_{n-1} + 2\sum_{j=0}^{w-1}\widehat{f}_{w-1-j}\widehat{f''}_j - f'^2_{n-1}$$
$$-\beta_1\mathrm{Re}\left(\frac{\sum_{j=0}^{w-1}\widehat{f}^2_{w-1-j}\widehat{f''}_j}{\eta} + 2\sum_{j=0}^{w-1}\widehat{f}^2_{w-1-j}\widehat{f'''}_j - 4\sum_{j=0}^{w-1}\widehat{f}^2_{w-2-j}\widehat{f'}_{w-1-j}\widehat{f''}_j\right)$$
$$- M\left(\widehat{f'}_{n-1} - \beta_1\sum_{j=0}^{w-1}\widehat{f}_{w-1-j}\widehat{f''}_j\right) + \lambda\left(\widehat{\theta'} + N_r\widehat{\phi}\right)$$

(28)

$$\Re_n^{\widehat{\theta}}(\eta) = (2\gamma\eta + 1)\widehat{\theta''}_{n-1} + \mathrm{Pr}\sum_{j=0}^{w-1}\widehat{\theta'}_{w-1-j}\hat{f}_j + \mathrm{Pr}N_b(2\gamma\eta + 1)_0\sum_{j=0}^{w-1}\widehat{\phi'}_{w-1-j}\widehat{\theta'}_j$$
$$+ \mathrm{Pr}M\left(Ec_1\widehat{f'^2}_{n-1} + Ec_2\widehat{g}_{n-1}\right) + \delta\mathrm{Pr}\mathrm{Re}\widehat{\theta}_{n-1} + \mathrm{Pr}N_t(2\gamma\eta + 1)\theta'^2_{n-1}$$

(29)

$$\Re_n^{\widehat{\phi}}(\eta) = (2\gamma\eta + 1)\widehat{\phi''}_{n-1} + Sc\sum_{j=0}^{w-1}\widehat{f}_{w-1-j}\widehat{\phi'}_j + 2\gamma\widehat{\theta'}_{n-1} + \frac{N_t}{N_b}\left[(2\gamma\eta + 1)\widehat{\theta''}_{n-1} + 2\gamma\widehat{\theta'}_{n-1}\right]$$ (30)

$$\text{While}\quad \chi_n = \begin{cases} 0, & \text{if } \zeta \leq 1 \\ 1, & \text{if } \zeta > 1. \end{cases}$$ (31)

Convergence analysis. To use HAM we need to find out solutions in series for velocity, temperature and concentration functions. In determination of these solutions, the auxiliary parameters h_f, h_θ and h_ϕ are encountered which are dependable for convergence of solution. To check the region of validity for these parameters,we have constructed h-curves at 10th order of approximation (see Figs. 2, 3, 4). From these figures we have noticed that the range for convergence is $-3.5 \leq h_f \leq 0$, $-3.0 \leq h_\theta \leq 0.5$ and $-2.0 \leq h_\phi \leq 0.1$. Moreover, Fig. 5 shows the residual errors of the HAM solution for various values of h.

Results and discussion
This work describes the mixed convection flow for Maxwell nanofluid with transfer of thermal energy over a stretching and rotating cylinder. The behaviors of different substantial parameters have been examined and discussed graphically. Numerical tables are also constructed to discuss impact of these parameters upon various profiles of flow system.

Flow characteristics. This subsection describes the impact of various physical parameters upon flow characteristics. These parameters include $\beta_1 = $ Maxwell parameter, $\gamma = $ curvature parameter, $\lambda = $ mixed convection parameter, $M = $ Hartman number, $N_r = $ Buoyancy ratio and Re $= $ Reynolds number as shown in Figs. 6, 7, 8, 9, 10, 11. From Fig. 6 we see that velocity reduces with larger values of β_1. Actually enhancing values of β_1 boost
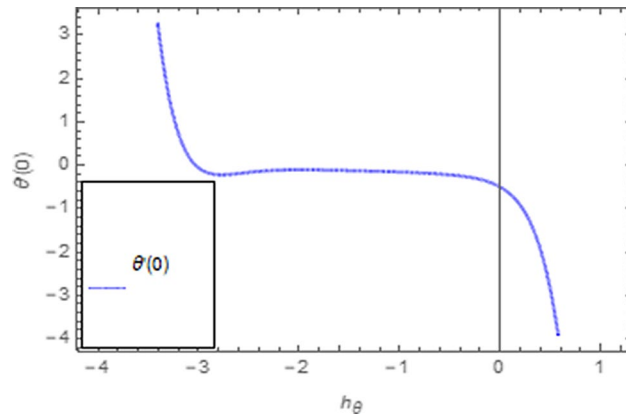
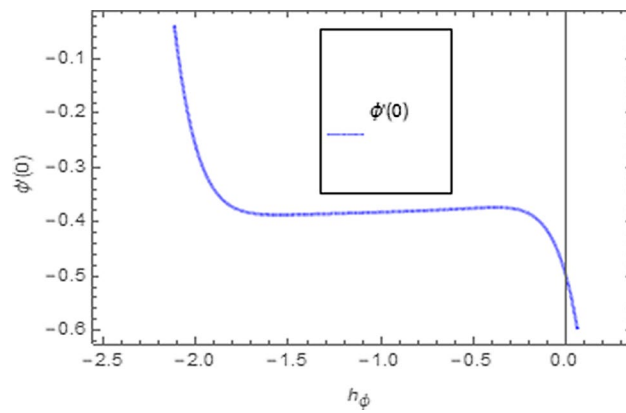**Figure 3.** $h-$ curve for $\theta(\eta)$.
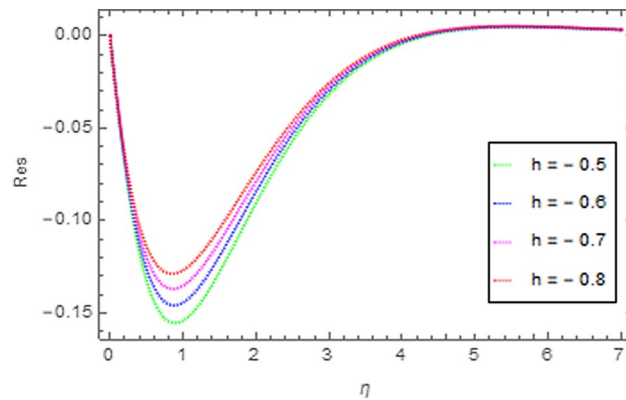

Figure 4. $h-$ curve for $\phi(\eta)$.

Figure 5. Residual errors sketch for solution using 10th order HAM approximation.

up the stress relaxation phenomenon, as a result of which flow characteristics of nanofluid declines. Figure 7 depicts impact of γ upon velocity. Since for γ to be higher, the radius of cylinder augments, ultimately fluid flow enhances. Figure 8 describes impact of λ on fluid flow. Here it is obvious that increasing values of λ, increase fluid flow. Actually with augmentation in mixed convection parameter, buoyancy forces increase as a result of this physical phenomenon there is a corresponding growth in flow characteristics of nanofluid. Impact of Hartman number upon velocity depicts in Fig. 9. Since when intensity of magnetic field increases it generates a resistive force in opposite direction of flow. Therefore, higher values of M decline velocity distribution of nanofluid. Impact of Buoyancy ratio upon flow of fluid is depicted in Fig. 10. It is understood that growth in N_r results in an augmentation in velocity distribution. Impact of Reynolds number on velocity profile portrays in Fig. 11.
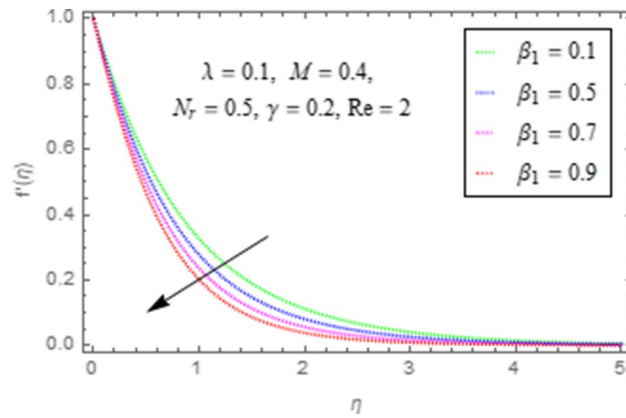
Figure 6. Impact of β_1 upon $f'(\eta)$.
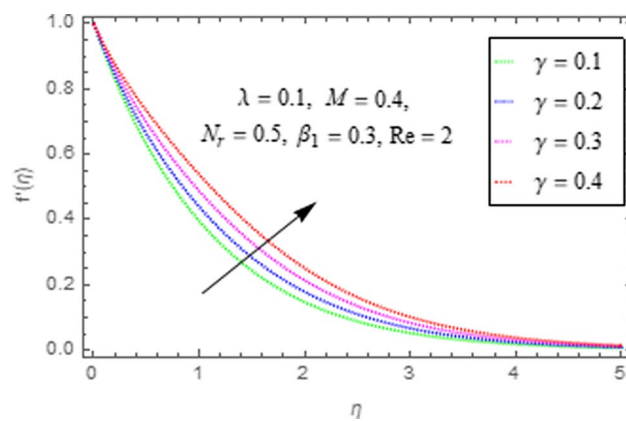
Figure 7. Impact of γ upon $f'(\eta)$.
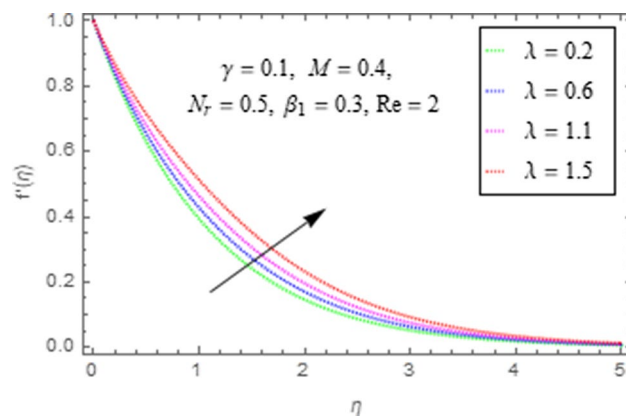
Figure 8. Impact of λ upon $f'(\eta)$.

Thisfigure describes that growing values of (Re) results in decliningof flow field. Physically it can be interpreted as, with growing values Reynolds number the inertial force of nanoparticles increases. Now since inertial force is an opposing agent for fluid flow of nanoparticles, hence motion of the fluid decreases.

Thermal characteristics. This subsection describes impact of Ec_1 = Eckert number for cylinder's stretching, Ec_2 = Eckert number for cylinder's rotation, N_b = Brownian motion parameter, N_t = Thermophoresis parameter, Pr = Prandtl number, Re = Reynolds number, γ = curvature parameter and δ = Heat generation/absorption parameter upon thermal characteristics of nanofluid as highlighted in Figs. 12, 13, 14, 15, 16, 17,
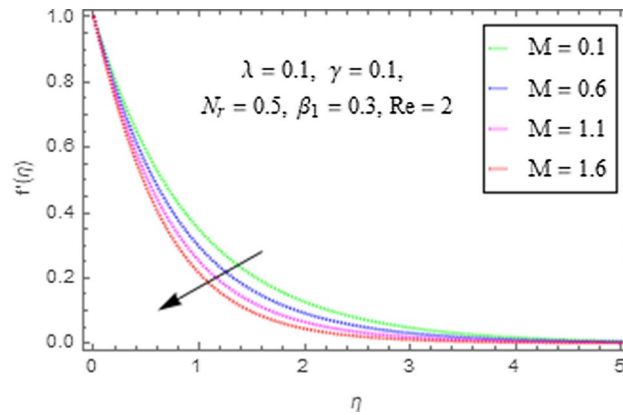
Figure 9. Impact of M upon $f'(\eta)$.
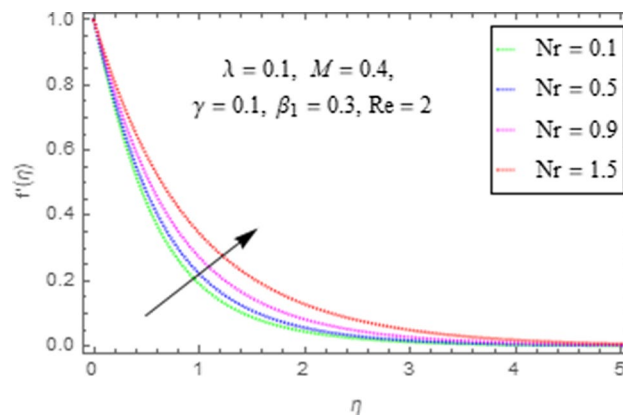
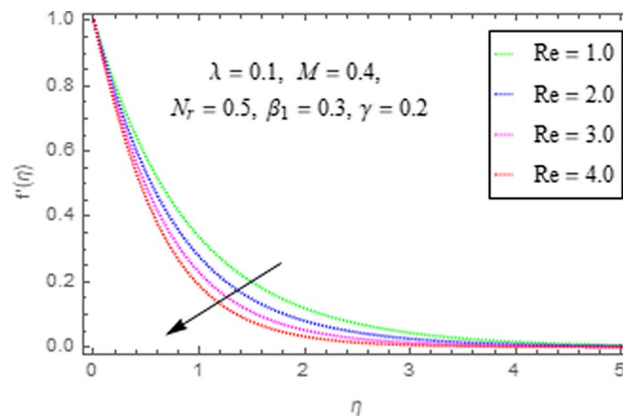**Figure 10.** Impact of Nr upon $f'(\eta)$.

Figure 11. Impact of Re upon $f'(\eta)$.

18, 19, 20. The impact of Eckert numbers (both used for stretching and rotation of cylinder) upon temperature is depicted in Figs. 12, 13. From these figures it is observed that due to enhancement in Eckert number there is a growth in thermal energy transportation of Maxwell nanofluid. Since Ec (ratio of kinetic energy to thermal energy transport driving force) represents Joule heating effects.Therefore, augmentation in Ec enhances temperature of nanofluid. Figure 14 depicts effect of N_b upon temperature. Since for growth in N_b there is a corresponding augmentation in random motion ofnanoparticles. This increase in random motion results in increasing the collision of nanoparticles, due to which kinetic energy is transformed to heat. Therefore, for augmentation in N_b there is an increase in temperature distribution of fluid. Impact of Thermophoresis parameter N_t upon temperature depicts in Fig. 15. Since $N_t = \frac{\tau D_T \Delta T}{T_\infty \upsilon}$, so increase in thermophoresis parameter means
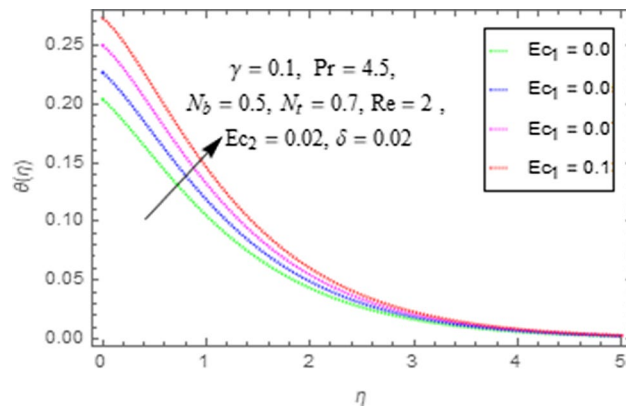
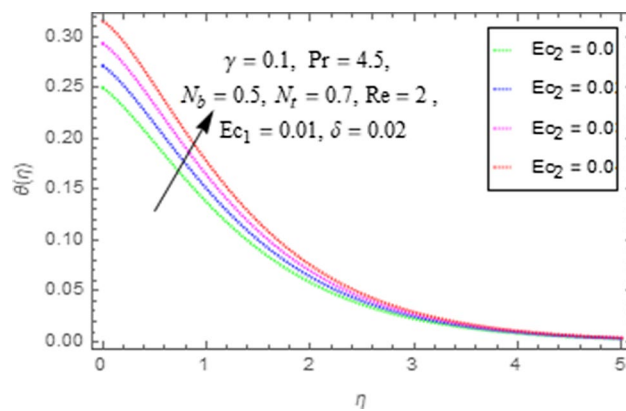**Figure 12.** Impact of Ec_1 upon $\theta(\eta)$.

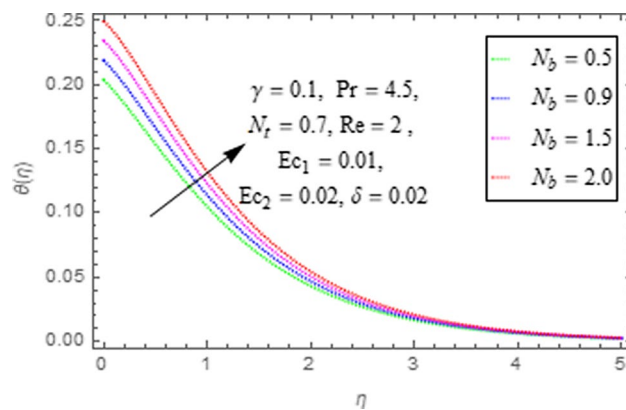**Figure 13.** Impact of Ec_2 upon $\theta(\eta)$.

Figure 14. Impact of N_b upon $\theta(\eta)$.

augmentation in temperature gradient. So for higher values of N_t we have corresponding growth in temperature. Impact of Prandtl number upon temperature is discussed in Fig. 16. We see that temperature decreases with augmentation inPrandtl number. Actually when Prandtl number increases, then mass as well as thermal diffusivity of nanoparticles reduceand henceits temperature reduces. Figure 17 depicts impact of Reynolds number over temperature distribution. Since increasing values of *Re* results in a reduction of convection force of nanoparticles and hence there is an increase in thermal characteristics of nanoparticles. Figure 18 depicts impact of curvature parameter γ on $\theta(\eta)$. We see that temperature augments with growing values of curvature parameter. Impact of δ upon temperature depicts in Figs. 19, 20 both for $\delta > 0$, $\delta < 0$. Since for heat source $\delta > 0$ we see that some additional heat is produced, that enhances heat transport properties of flow system, hence temperature of system
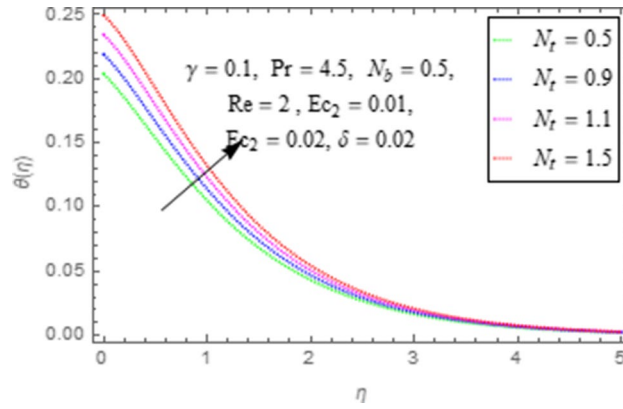
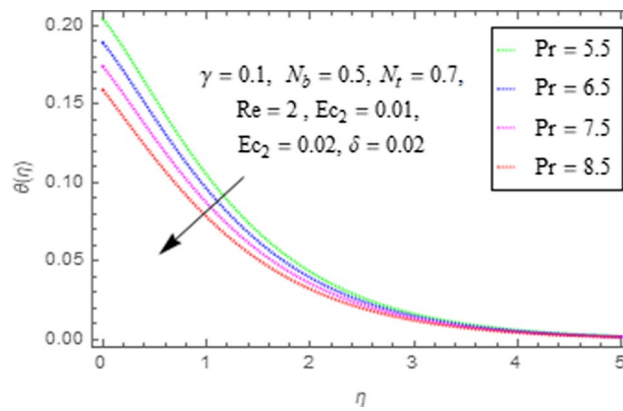**Figure 15.** Impact of N_t upon $\theta(\eta)$.

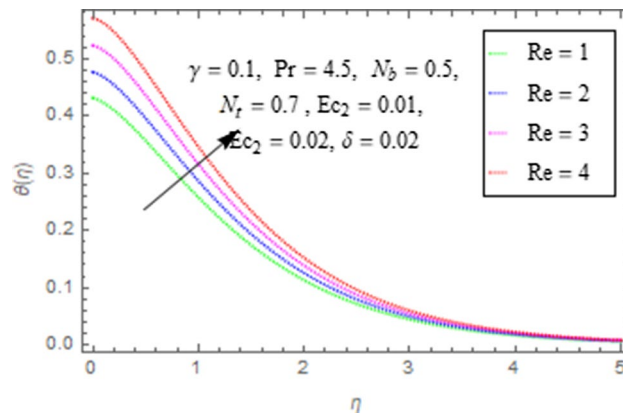**Figure 16.** Impact of Pr upon $\theta(\eta)$.

Figure 17. Impact of Re upon $\theta(\eta)$.

enhances in this case as shown in Fig. 19. Moreover, a reverse impact is observed for heat sink $\delta < 0$. Actually for $\delta < 0$ the transport characteristics of flow system reduces that ultimately reduces temperature of nanofluid as shown in Fig. 20.

Concentration characteristics. This subsection describes impact of $N_b =$ Brownian motion parameter, $N_t =$ Thermophoresis parameter and $Sc =$ Schmidt number upon concentration distribution $\phi(\eta)$ as given in Figs. 21, 22, 23. Figure 21 portrays effect of N_b upon $\phi(\eta)$. It is obvious from this figure that concentration of
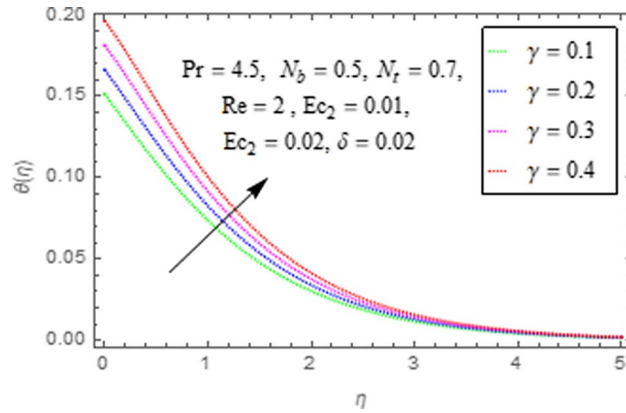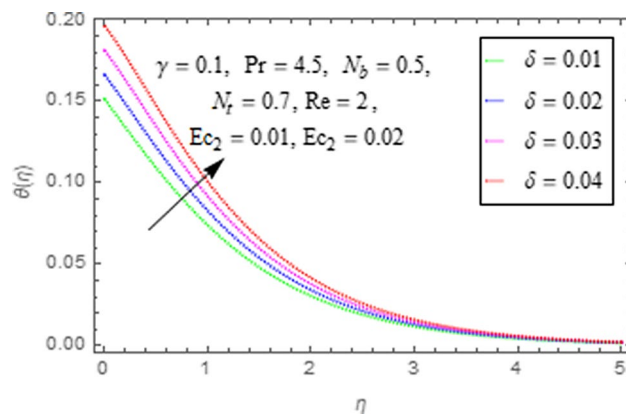
Figure 18. Impact of γ upon $\theta(\eta)$.

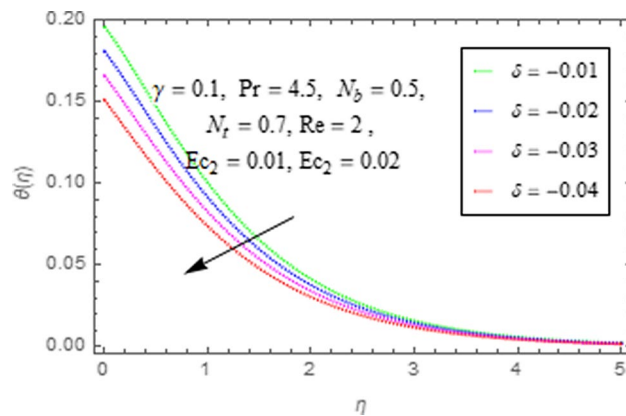**Figure 19.** Impact of δ upon $\theta(\eta)$.

Figure 20. Impact of (δ) upon $\theta(\eta)$.

nanofluid reduces for higher values of N_b. Actually Brownian motion is haphazard motion of nanoparticles (which are suspended in base fluid) and is more influenced by fast moving molecules. Figure 22 describes that with higher values of N_t, the concentration of fluid grows up. In fact when N_t increases then temperature differences between wall and free surface also increases that ultimately enhances concentration of nanofluid. Fi 23 depicts impact of Schmidt number upon concentration distribution. From this figure it is determined that enhancing values of Sc reduces concentration of nanofluid. In fact, when Sc increases then molecular/mass diffusivity of fluid reduces that ultimately reduces the concentration of nanoparticles as shown in Fig. 23.
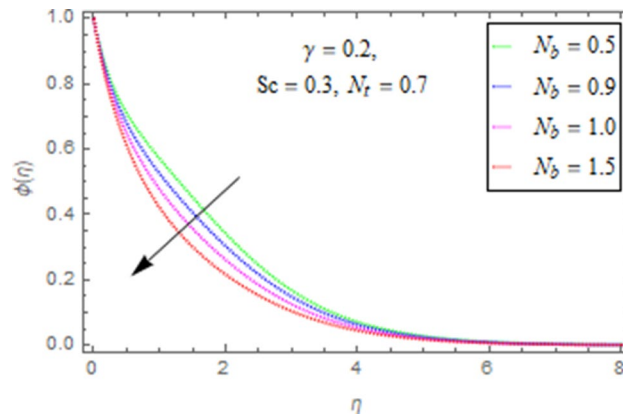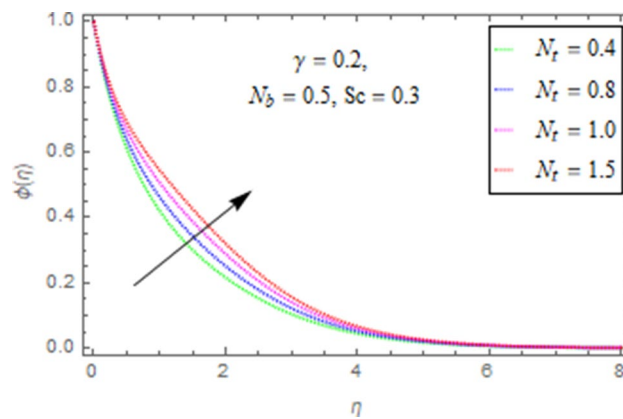
Figure 21. Impact of N_b upon $\phi(\eta)$.

Figure 22. Impact of N_t upon $\phi(\eta)$.
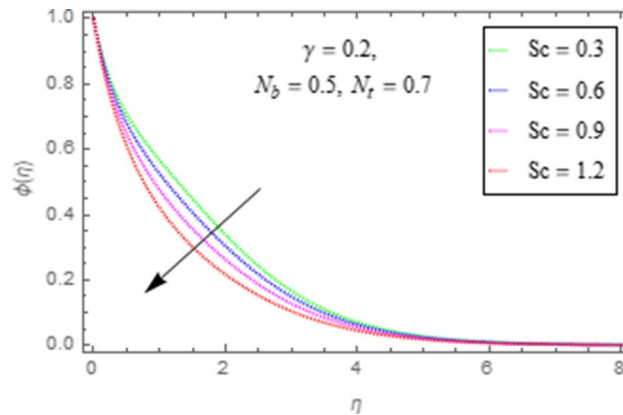
Figure 23. Impact of Sc upon $\phi(\eta)$.

Table discussion. The numerical values for different substantial parameters upon velocity profile, temperature gradient and concentration gradient are evaluated in Tables 1, 2 and 3 respectively. Moreover, a comparison is also carried out for validation of current work with the results as available in literature[46]. It is observed from this comparison that our result is in good conformity with the filed values which are presented in Table 4.

Re	γ	$\beta1$	M	$f(\eta)$	$f'(\eta)$
0.1	0.23	0.31	0.25	0.8313793	0.1306459
0.2				0.8258029	0.1280804
0.3				0.8202604	0.1255435
	0.1			0.8263999	0.1238384
	0.2			0.8302507	0.1306459
	0.3			0.8339640	0.1370183
		0.1		0.8398284	0.1365566
		0.2		0.8357958	0.1345714
		0.3		0.8317799	0.1326024
			0.1	0.8573742	0.1440031
			0.2	0.8399046	0.1361867
			0.3	0.8229916	0.1287101

Table 1. Impact of various substantial parameters over velocity profiles $f(\eta)$ and $f'(\eta)$.

δ	γ	Pr	Ec1	Ec2	M	$\theta(\eta)$
0.3	0.23	0.31	0.25	0.29	0.15	0.0911114
0.4						0.0918603
0.5						0.0926147
	0.3					0.0938488
	0.4					0.0976639
	0.5					0.1013696
		0.3				0.0907708
		0.4				0.0941896
		0.5				0.0976367
			0.3			0.0917239
			0.4			0.0929489
			0.5			0.0941740
				0.3		0.0911394
				0.4		0.0914196
				0.5		0.0917006
					0.3	0.0948719
					0.4	0.0973467
					0.5	0.0997969

Table 2. Impact of various substantial parameters over temperature $\theta(\eta)$.

γ	Sc	$\phi(\eta)$
0.5	0.45	0.0347714
0.6		0.0292947
0.7		0.0240052
0.37	0.5	0.0417823
	0.6	0.0409927
	0.7	0.0402080

Table 3. Impact of over concentration $\phi(\eta)$ various substantial parameters.

Conclusions

This work describes the mixed convection flow for Maxwell nanofluid with transfer of thermal energy over a stretching and rotating cylinder in the presence of Joule heating and Heat generation/absorption. The modeled problem is solved by HAM.The behaviors of different substantial parameters have been examined and discussed graphically. Tables are also constructed to see numerically the impact of different substantial parameters upon flow characteristics.Moreover, a comparison is also carried out for validation of current work with the results as

γ	N_b	N_t	γ_1	γ_2	$Nu_z(\mathrm{Re}_z)^{-1/2}$		$Sh_z(\mathrm{Re}_z)^{-1/2}$	
					Ref.[46]	Present work	Ref.[46]	Present work
0.1	0.1	0.1	0.2	0.7	0.15571	0.155721	0.28856	0.288572
0.2					0.15712	0.157130	0.29877	0.298784
0.3					0.15839	0.158402	0.30942	0.309439
0.1	0.2				0.15459	0.154603	0.31332	0.313337
	0.3				0.15352	0.153531	0.32173	0.321746
	0.4				0.15243	0.152440	0.32602	0.326039
	0.1	0.2			0.15553	0.155543	0.24168	0.241691
		0.3			0.15532	0.155334	0.19622	0.196230
		0.4			0.15513	0.155142	0.15235	0.152367
		0.1	0.5		0.29332	0.293337	0.25090	0.250919
			0.7		0.35292	0.352936	0.23510	0.235116
			0.9		0.39792	0.397938	0.22329	0.223391
			0.2	0.5	0.15578	0.155791	0.24135	0.241365
				0.8	0.15569	0.155691	0.30742	0.307436
				1.0	0.15563	0.155640	0.33836	0.338374

Table 4. Comparison between present result and Ref.[46] for Nusselt and Sherwood numbers at different values of substantial parameters $\gamma,\ N_b,\ N_t,\ \gamma_1\ and\ \gamma_2$.

available in literature[46]. It is observed from this comparison that our result is in good agreement with the filed values. After detailed study of the article the following observations have been noticed:

- Enhancing values of Maxwell parameter boost up the stress relaxation phenomenon, as a result of which flow characteristics of nanofluid reduces.
- Increase in mixed convection parameter increases buoyancy forces due to this physical phenomenon, flow characteristics of nanofluid also increase.
- Rise in intensity of magnetic field, generates Lorentz forces that produces a resistive force in reverse direction of flow field and ultimately declines velocity distribution of nanofluid.
- It is observed that due to enhancement in Eckert number there is an increase in thermal energy transportation of Maxwell nanofluid.
- Increase in Brownian motion of nanoparticles, converts kinetic energy into heat energy, that ultimately increases temperature.
- Increase in thermophoresis parameter, increases temperature gradient that result in augmentation of nanoparticles temperature.
- With augmentation in Prandtl number, the mass as well as thermal diffusivities of nanoparticles reduce, as an outcome of which warmth of fluid reduces.
- For heat source $\delta > 0$, some additional heat is produced, that enhances heat transport properties of flow system and hence temperature of system enhances in this case. A reverse impact has seen for heat sink $\delta < 0$.
- When thermophoresis parameter increases then temperature differences between wall and free surface also increases that ultimately enhances concentration of nanofluid.
- For elevated values of Schmidt numbert hemolecular/mass diffusivity of fluid reduces, that ultimately reduces the concentration of nanoparticles.

References

1. Choi, S. U. S. Enhancing thermal conductivity of fluids with nanoparticle. *ASME Int. Mech. Eng. Cong. Expo.* **66**, 99–105 (1995).
2. Ellahi, R., Hassan, M., Zeeshan, A. & Khan, A. A. The shape effects of nanoparticles suspended in HFE-7100 over wedge with entropy generation and mixed convection. *Appl. Nanosci.* **6**, 641–651 (2016).
3. Dogonchi, A. S. & Ganji, D. D. Thermal radiation effect on the nanofluid buoyancy flow and heat transfer over a stretching sheet considering Brownian motion. *J. Mol. Liq.* **223**, 521–527 (2016).
4. Dogonchi, A. S. & Ganji, D. D. Analytical solution and heat transfer of two-phase nanofluid flow between non-parallel walls considering Joule heating effect. *Powder Technol.* **318**, 390–400 (2017).
5. Kumar, R., Seth, G. S. & Bhattacharyya, A. Entropy generation of von Karman's radiative flow with Al2O3 and Cu nanoparticles between two coaxial rotating disks: A finite-element analysis. *Eur. Phys. J. Plus* **134**(12), 597 (2019).
6. Gul, M., Abbasi, F. M., Shehzad, S. A. & Shafee, A. Entropy generation for peristaltic motion of Carreau's fluid with mixture of ethylene glycol and boron-nitride nanoparticles. *PhysicaScripta* **95**(3), 035212 (2020).
7. Abbasi, F. M., Shanakhat, I. & Shehzad, S. A. Entropy generation analysis for peristalsis of nanofluid with temperature dependent viscosity and Hall effects. *J. Magn. Magn. Mater.* **474**, 434–441 (2019).

8. Waqas, M., Shehzad, S. A., Hayat, T., Khan, M. I. & Alsaedi, A. Simulation of magnetohydrodynamics and radiative heat transport in convectively heated stratified flow of Jeffrey nanofluid. *J. Phys. Chem. Solids* **133**, 45–51 (2019).
9. Mukhopadhyay, S. Effects of slip on unsteady mixed convective flow and heat transfer past a porous stretching surface. *Nucl. Eng. Des.* **241**(8), 2660–2665 (2011).
10. Hayat, T., Shehzad, S. A., Alsaedi, A. & Alhothuali, S. M. Mixed convection stagnation point flow of casson fluid with convective boundary conditions. *Chin. Phys. Lett.* **29**(11), 114704 (2012).
11. Turkyilmazoglu, M. The analytical solution of mixed convection heat transfer and fluid flow of a MHD viscoelastic fluid over a permeable stretching surface. *Int. J. Mech. Sci.* **77**, 263–268 (2013).
12. Shehzad, S. A., Alsaedi, A., Hayat, T. & Alhuthali, M. S. Thermophoresis particle deposition in mixed convection three-dimensional radiative flow of an Oldroyd-B fluid. *J. Taiwan Inst. Chem. Eng.* **45**(3), 787–794 (2014).
13. Xu, H. & Pop, I. Mixed convection flow of a nanofluid over a stretching surface with uniform free stream in the presence of both nanoparticles and gyrotactic microorganisms. *Int. J. Heat Mass Transf.* **75**, 610–623 (2014).
14. Sankar, M., Park, Y., Lopez, J. M. & Do, Y. Numerical study of natural convection in a vertical porous annulus with discrete heating. *Int. J. Heat Mass Transf.* **54**(7–8), 1493–1505 (2011).
15. Sankar, M., Kiran, S., Ramesh, G. K. & Makinde, O. D. Natural convection in a non-uniformly heated vertical annular cavity. *Defect Diffus. Forum* **377**, 189–199 (2017).
16. Sankar, M. & Do, Y. Numerical simulation of free convection heat transfer in a vertical annular cavity with discrete heating. *Int. Commun. Heat Mass Transfer* **37**(6), 600–606 (2010).
17. Jagadeesha, R. D., Prasanna, B. M. R. & Sankar, M. Double diffusive convection in an inclined parallelogrammic porous enclosure. *Procedia Eng.* **127**, 1346–1353 (2015).
18. Sankar, M., Jang, B. & Do, Y. Numerical study of non-Darcy natural convection from two discrete heat sources in a vertical annulus. *J. Porous Media.* **17**, 373–390 (2014).
19. Sankar, M., Park, J., Kim, D. & Do, Y. Numerical study of natural convection in a vertical porous annulus with an internal heat source: Effect of discrete heating. *Numer. Heat Transf. Part A Appl.* **63**(9), 687–712 (2013).
20. Mustafa, M., Hayat, T. & Obaidat, S. On heat and mass transfer in the unsteady squeezing flow between parallel plates. *Meccanica* **47**, 1581–1589 (2012).
21. Kumari, M. & Nath, G. Analytical solution of unsteady three-dimensional MHD boundary layer flow and heat transfer due to impulsively stretched plane surface. *Commun. Nonlinear Sci. Numer. Simul.* **14**(8), 3339–3350 (2009).
22. Alizadeh, M., Dogonchi, A. S. & Ganji, D. D. Micropolarnanofluid flow and heat transfer between penetrable walls in the presence of thermal radiation and magnetic field. *Case Stud. Therm. Eng.* **12**, 319–332 (2018).
23. Ashorynejad, H. R., Sheikholeslami, M., Pop, I. & Ganji, D. D. Nanofluidflow and heat transfer due to a stretching cylinder in the presence of magnetic field. *Heat Mass Transf.* **49**(3), 427–436 (2013).
24. Seth, G. S., Kumar, R., Tripathi, R. & Bhattacharyya, A. Double diffusive MHD Casson fluid flow in a non-Darcy porous medium with Newtonian heating and thermo-diffusion effects. *Int. J. Heat Technol.* **36**(4), 1517–1527 (2018).
25. Seth, G. S., Bhattacharyya, A., Kumar, R. & Mishra, M. K. Modeling and numerical simulation of hydromagnetic natural convection Casson fluid flow with nth-order chemical reaction and Newtonian heating in porous medium. *J. Porous Media.* **22**(9), 1141–1157 (2019).
26. Tripathi, R., Seth, G. S. & Mishra, M. K. Double diffusive flow of a hydromagneticnanofluid in a rotating channel with Hall effect and viscous dissipation: Active and passive control of nanoparticles. *Adv. Powder Technol.* **28**(10), 2630–2641 (2017).
27. Arifuzzaman, S. M. *et al.* Hydrodynamic stability and heat and mass transfer flow analysis of MHD radiative fourth-grade fluid through porous plate with chemical reaction. *J. King Saud Univ. Sci.* **31**(4), 1388–1398 (2019).
28. Crane, L. J. Flow past a stretching plate. *J. Appl. Math. Phys.* **21**, 645–647 (1970).
29. Wang, C. Y. & Ng, C. O. Slip flow due to a stretching cylinder. *Int. J. Non-Linear Mech.* **46**, 1191–1194 (2011).
30. Bhattacharyya, A., Seth, G. S., Kumar, R. & Chamkha, A. J. Simulation of Cattaneo-Christov heat flux on the flow of single and multi-walled carbon nanotubes between two stretchable coaxial rotating disks. *J. Therm. Anal. Calorim.* **139**(3), 1655–1670 (2020).
31. Seth, G. S., Bhattacharyya, A., Kumar, R. & Chamkha, A. J. Entropy generation in hydromagneticnanofluid flow over a non-linear stretching sheet with Navier's velocity slip and convective heat transfer. *Phys. Fluids* **30**(12), 122003 (2018).
32. Ahmmed, S. F., Arifuzzaman, S. M., Sarkar, T. & Khan, M. Computational modelling of multiphase fluid flow behaviour over a stretching sheet in the presence of nanoparticles. *Eng. Sci. Technol. Int. J.* **23**(3), 605–617 (2019).
33. Reza-E-Rabbi, S., Arifuzzaman, S. M., Sarkar, T., Khan, M. S. & Ahmmed, S. F. Explicit finite difference analysis of an unsteady MHD flow of a chemically reacting Casson fluid past a stretching sheet with Brownian motion and thermophoresis effects. *J. King Saud Univ. Sci.* **32**(1), 690–701 (2020).
34. Rana, B. M. J., Arifuzzaman, S. M., Reza-E-Rabbi, S., Ahmed, S. F. & Khan, M. S. Energy and magnetic flow analysis of Williamson micropolarnanofluid through stretching sheet. *Int. J. Heat Technol.* **37**(2), 487–496 (2019).
35. Ahmmed, S. F., Arifuzzaman, S. M., Sarkar, T. & Khan, M. Computational modelling of multiphase fluid flow behavior over a stretching sheet in the presence of nanoparticles. *Eng. Sci. Technol. Int. J.* **23**(3), 605–617 (2020).
36. Seth, G. S., Sharma, R., Mishra, M. K. & Chamkha, A. J. Analysis of hydromagnetic natural convection radiative flow of a viscoelastic nanofluid over a stretching sheet with Soret and Dufour effects. Eng. Comput. (2017).
37. Seth, G. S., Bhattacharyya, A. & Mishra, M. K. Study of partial slip mechanism on free convection flow of viscoelastic fluid past a nonlinearly stretching surface. *Comput. Therm. Sci.* **11**, 107–119 (2018).
38. Liao,S.J. The proposed homotopy analysis method for the solution of nonlinear problems, PhD Thesis, Shangai Jiao Tong University (1992).
39. Shehzad, S. A. Magnetohydrodynamic Jeffrey nanoliquid flow with thermally radiative Newtonian heat and mass species. *Revistamexicana de física* **64**(6), 628–633 (2018).
40. Ahmad, M., Shehzad, S. A., Iqbal, A. & Taj, M. Time-dependent three-dimensional Oldroyd-B nanofluid flow due to bidirectional movement of surface with zero mass flux. *Adv. Mech. Eng.* **12**(4), 1-12 (2020).
41. Bhattacharyya, K. MHD stagnation point flow of Casson fluid and heat transfer over a stretching sheet with thermal radiation. *J. Thermodyn.* 1–9 (2013).
42. Mukhopadhyay, S. Casson fluid flow and heat transfer over a nonlinearly stretching surface. *Chin. Phys. B.* **22**(7), 074701 (2013).
43. Pramanik, S. Casson fluid flow and heat transfer past an exponentially porous stretching surface in presence of thermal radiation. *Ain Shams Eng. J.* **5**(1), 205–212 (2014).
44. Mustafa, M., Hayat, T., Pop, I. & Hendi, A. Stagnation-point flow and heat transfer of a Casson fluid towards a stretching sheet. *Z. Naturforsch.* **67a**, 70–76 (2012).
45. Eastman, J. A., Choi, S. U. S., Li, S., Yu, W. & Thompson, L. J. Anomalously increased effective thermal conductivity of ethylene glycol-based nanofluids containing copper nanoparticles. *Appl. Phys. Lett.* **78**(6), 718–720 (2001).
46. Imtiaz, M., Hayat, T. & Alsaedi, A. Mixed convection flow of Cassonnanofluid over a stretching cylinder with convective boundary conditions. *Adv. Powder Technol.* **27**(5), 2245–2256 (2016).

Acknowledgements

Author contributions

A.K., Z.S. and P.K. modeled and solved the problem. A.K. and S.I. wrote the manuscript. S.I., M.Z. W.K. and M.J. contributed in the numerical computations and plotting the graphical results. H.R. and W.K. contributed in the revesion. All the authors finalized the manuscript after its internal evaluation.

Competing interests

The authors declare no competing interests.

Additional information

Correspondence and requests for materials should be addressed to P.K. or Z.S.

Reprints and permissions information is available at www.nature.com/reprints.

Publisher's note Springer Nature remains neutral with regard to jurisdictional claims in published maps and institutional affiliations.